An Experimental and Numerical Study of Flow and Convective Heat Transfer in a Freely Falling Curtain of Particles

J. Hruby
R. Steeper
G. Evans
C. Crowe

Sandia National Laboratories, Livermore, Livermore, Calif., Washington State University, Pullman, Wash.

The flow characteristics and convective heat transfer in a freely falling curtain of spherical particles with an average diameter of 650 μm has been studied experimentally and numerically. Both heated and unheated particle flows have been considered. This work is part of a larger study to determine the feasibility of using particles to directly absorb the insolation in a solar central receiver for high temperature applications. The particles of interest are Norton Master Beads™ which are primarily aluminum oxide. Measurements have been made of particle velocity in heated and unheated particle flows, and particle temperature and air temperature in heated particle flows. Comparison of the measurements with calculations has been made for two particle mass flow rates at room temperature and at two initial elevated particle temperatures. Excellent agreement between numerical and experimental results is obtained for particle velocity in the unheated flow. For the heated particles, both data and predictions show the same trends with regard to particle velocity, particle temperature, and air temperature. However, the calculations of these quantities overpredict the data. The results suggest that the drag coefficient in flows where the particles are hot compared to the air is larger than predicted using conventional methods to account for nonisothermal effects. The prediction of particle temperature and air temperature attained with a drag coefficient that is larger than the standard drag coefficient agrees well with the data.

Introduction

The flow characteristics and convective heat transfer in a freely falling curtain of particles have been investigated experimentally and numerically. This work is part of a larger study to determine the feasibility of using particles as direct absorbers of the insolation in a solar central receiver.

A solar central receiver system uses mirrors to reflect and focus sunlight onto a receiver located on top of a tower. By redirecting the sunlight in this manner, the solar flux at the receiver surface can be equivalent to hundreds of suns. A working medium heated in the receiver can be used to produce electricity, or incorporated into products as process heat. Currently, the working media in solar central receivers are gases or liquids which flow through tubes heated by the solar radiation. An example of such a system is the water/steam central receiver system located near Barstow, California, which produces electrical energy (Radosevich, 1985). Other common working fluids include molten salts, molten metals, and air.

The concept of interest here, termed the solid particle receiver, employs sand-size refractory particles which free-fall in a solar receiver and directly absorb the solar insolation (Martin and Vitko, 1982 and Hruby, 1986b). A conceptual design of a solid particle receiver is shown in Fig. 1. The solid particle receiver is being evaluated for high temperature (greater than 550°C) applications of solar energy. The advantages of a solid particle receiver over traditional fluid-in-tube receivers are: (1) the particles can directly absorb solar radiation eliminating thermal fatigue limitations on tube materials, and (2) the particles have high volumetric heat capacities and maintain their integrity at high temperatures. These advantages, coupled with the possibility that the particles can serve as the storage medium, could enable the solid particle receiver to be a cost effective means of high temperature solar energy utilization. High temperatures are attractive for fuels and chemicals production, industrial process heat applications, and Brayton cycle electricity generation.

In order to evaluate the performance of solid particles as the working media in a central receiver system, the behavior of freely falling particle curtains must be understood. The air-particle flow is expected to be dilute in the receiver. Dilute flow implies that the particle velocity is controlled by the aerodynamic drag and the gravitational force, not by particle-particle collisions. This report presents experimental data and

Contributed by the Fluids Engineering Division for publication in the JOURNAL OF FLUIDS ENGINEERING. Manuscript received by the Fluids Engineering Division January 28, 1987.

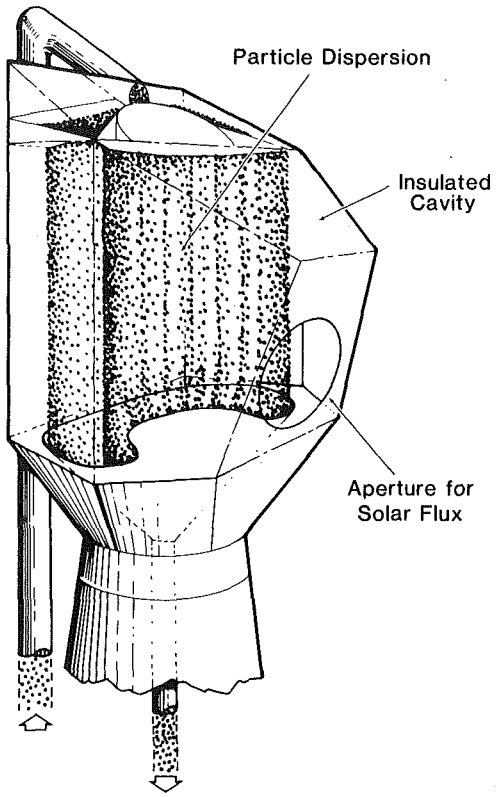

Fig. 1 Conceptual design of a solid particle central receiver

numerical predictions of the aerodynamic and thermal behavior of heated and unheated particles freely falling in initially quiescent air at room temperature. Other experimental studies of dilute freely falling particle curtains for the solid particle receiver project include the development of a particle velocity measurement system (Hruby and Burolla, 1984) and an experiment in which the particles were heated with a radiant flux (Burolla, Hruby, and Steele, 1984). Numerical work has focused on developing a model of a solid particle solar central receiver including radiative transfer within the particle cloud (Houf and Greif, 1985), and including the two phase flow and heat transfer of air and particles within the cavity receiver (Evans et al., 1986a). This model also accounts for convection and radiation from the walls of the cavity.

The numerical and experimental work performed previously has demonstrated the importance of two-way coupling between the particles and the air. Both measured and predicted velocities in the curtain were higher than the velocity of an isolated sphere in free-fall. The higher particle velocity is the result of entrainment of the surrounding air by the particle curtain, and can only be predicted with two-dimensional modeling and momentum coupling between the air and particle phase (Evans et al., 1986b). The previous work has also shown that coupling between momentum and energy is necessary for correct prediction of particle temperature. Momentum and energy coupling is important because the particle-air heat transfer can influence both particle velocity and particle temperature. The present experiment was designed to study particle velocity in both heated and unheated particle curtains, as well as particle temperature and air temperature in heated flows. The influence of initial particle temperature and mass flow rate was investigated.

Nomenclature

C_D = drag coefficient
F_p^x = drag force exerted on a single particle in the x-direction, N
$\dot{N}$ = particle number flow rate
Nu = Nusselt number $= hd_p/k$
P = pressure, N/m^2
Pr = Prandtl number
Q_p = heat transfer from a particle to air $=$ $\mathrm{Nu}k_f\,\pi d_p(T-T_p)$, W
Re = particle Reynolds number $= \rho d_p\,|\mathbf{u}_p-\mathbf{u}|/\mu$
$S_p^{x,y}$ = gas x, y momentum equation source term due to particles, N
S_p^T = gas energy equation source term due to particles, kg•K/s
T = temperature, K
T_g^* = dimensionless gas temperature $=$ $(T_g-T_\infty)/(T_{po}-T_\infty)$
T_p^* = dimensionless particle temperature $=$ $(T_p-T_\infty)/(T_{po}-T_\infty)$
T_{po} = initial particle temperature, K
T_∞ = ambient temperature, K
c_p = specific heat of air, J/(kg•K)
$c_{p_{part}}$ = specific heat of particle, J/(kg•K)
d_p = particle diameter, m or μm
g = acceleration due to gravity, m/s^2
h = convective heat transfer coefficient, W/(m^2•K)
k = thermal conductivity, W/(m•K)
n = particle number density, particles/m^3
t = time, s
Δt_i = particle transit time across a computational cell along the ith trajectory, s
u = vertical velocity, m/s
v = horizontal velocity, m/s
x = vertical position coordinate, m
y = horizontal position coordinate, m
Δx = vertical grid spacing, m
Δy = horizontal grid spacing, m
ϵ = particle emissivity or turbulent dissipation, m^2/s^2
κ = turbulent kinetic energy, m^2/s^2
σ = Stefan-Boltzmann constant = 5.669 E-08 W/(m^2•K^4)
ρ = density, kg/m^3
λ = ratio of $C_D/C_{D_{\mathrm{Stokes}}} = (\nu_f/\nu)\,(1+0.15\mathrm{Re}_f^{2/3})$
μ = dynamic viscosity, kg/(m•s)
ν = kinematic viscosity, m^2/s

Subscripts

eff = effective viscosity or conductivity
f = evaluated at the film temperature
g = gas phase
i = the ith trajectory
p = particle phase
s = surface
turb = turbulent quantity
n, s, e, w = values evaluated at north, south, east, or west faces of control volume
∞ = evaluated at ambient conditions

Superscripts

i = initial particle conditions
$*$ = nondimensional quantity
x, y = x- or y-direction

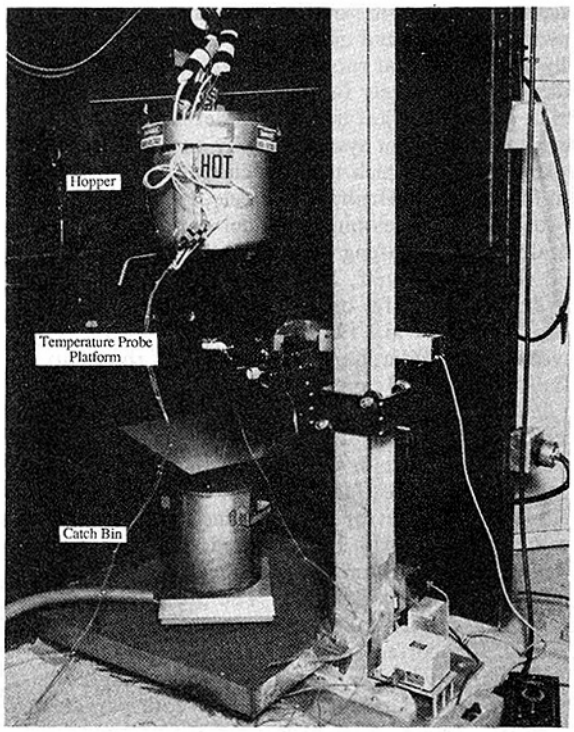

Fig. 2 Photograph of experimental apparatus identifying three assemblies: (1) hopper, (2) catch bin, and (3) temperature probe platform

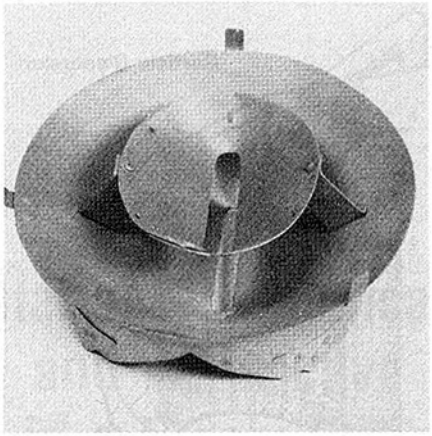

Fig. 3 Funnel-shaped inserts used in the hopper to provide a uniform temperature particle curtain at the hopper exit

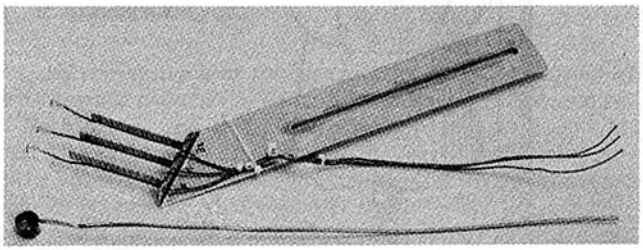

Fig. 4 Probes used to measure particle temperature and air temperature in the particle curtain

The calculations and experiments were performed using Norton Master Beads™ with an average size of 650 μm (94.6 percent between 417 and 710 μm and 5.4 percent between 250 and 417 μm). Master Beads™ are 86 percent aluminum oxide; the remaining 14 percent is comprised of near equal amounts of silica, iron oxide, and titania. Master Beads™ have been identified as particles that have high solar absorptivity, do not agglomerate at 1000°C, and have high fracture resistance (Hruby and Steele, 1986a).

Description of the Experiment

The experimental apparatus consisted of the following five assemblies: (1) hopper, (2) catch bin, (3) temperature probe platform, (4) laser Doppler velocimetry (LDV) system, and (5) data acquisition system. These assemblies are described in this section.

Hopper. The hopper (see Fig. 2) was a cylindrical, stainless steel receptacle that held 20 kg of heated Master Bead™ particles. The particles were discharged through an exit slit to form a steady, freely falling curtain. The hopper was suspended from a hoist and could be positioned from a few centimeters to 3.5 m above the catch bin assembly.

A uniform particle temperature at the hopper exit was obtained in the following manner. First, a convection oven was used to uniformly heat the particles prior to loading them in the hopper. Second, the hopper was ringed with band heaters controlled to maintain a constant interior wall temperature. Third, two funnel-shaped inserts (see Fig. 3) were stacked just above the exit slit to insure a uniform flow of particles within the hopper. It was observed that without these inserts, cooler particles from the top surface would funnel down the center and exit giving rise to a cool region within the curtain. Finally, three 1.6 mm shielded thermocouple probes were fixed vertically in the hopper with their tips 13 mm above the exit slit to record the temperature of the particles at this location.

The particle curtain was generated by a rectangular slit in the bottom plate of the hopper. The slit could be modified to provide two particle mass flow rates. For the low mass flow rate, the slit was covered with a 3.2 mm stainless steel screen. Slit dimensions in this case were 64 mm by 6.4 mm (aspect ratio of 10:1) and the particle mass flow rate was about 0.02 kg/s. For high mass flow rate, the screen was replaced with a single strand of 1.5 mm wire oriented longitudinally along the slit. With this arrangement, and slit dimensions of 51 mm by 5.1 mm, the particle mass flow rate was approximately 0.04 kg/s.

Catch Bin. The catch bin assembly, shown in Fig. 2, consisted of a funnel, an insulated receptacle, and an electronic scale platform. Falling particles were collected by the wide-mouthed funnel and channeled to the receptacle. The catch bin weight was successively measured by the scale to yield the particle mass flow rate.

Temperature Probe Platform. The probe platform, also shown in Fig. 2, was a moveable stage mounted on a vertical beam next to the particle curtain. It supported the temperature probes and could be positioned at any elevation from the hopper to the catch bin.

Two types of temperature probes, shown in Fig. 4, were used depending upon whether the particle temperature or air temperature was being measured. For measurement of particle temperature, a sampling cup consisting of a small, stainless steel foil cup fitted with a bare type K thermocouple junction was constructed. A hole was drilled in the bottom to allow a steady flow of particles past the junction when the cup was placed in the particle curtain. Several sizes and shapes were tried, the final choice being a short cylinder 10 mm high by 28 mm in diameter with a 3 mm hole in the bottom. Disturbance of the particle curtain by the sampling cup was small as shown in Fig. 5.

Air temperature was measured with a rake consisting of three bare type K thermocouples. The junction and last 7 mm of lead wire of each thermocouple were bent at right angles. When positioned in the curtain with the right angle section parallel to the flow and the junction downstream (see Fig. 6),

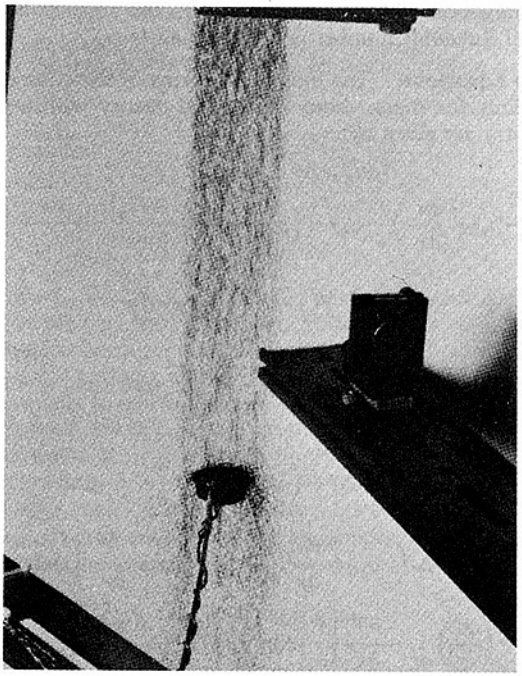

Fig. 5 Particle temperature sampling cup in the particle curtain during data collection

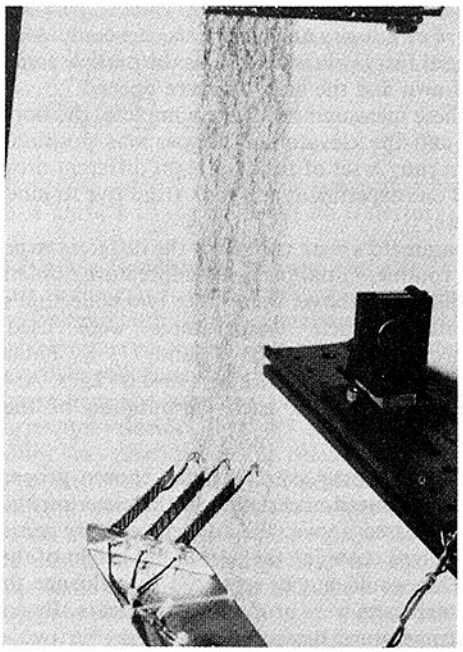

Fig. 6 Air temperature rake in the particle curtain during data collection

the thermocouples were shielded from contact with falling particles and so measured air temperatures. The three junctions were spaced 18 mm apart. The measurement of air temperature with thermocouple probes turned downstream has been performed successfully by others (Brewster and Seader, 1984).

A HeNe laser mounted on the elevator stage was used for visually positioning the stage with respect to reference marks on the wall. A linear position transducer was attached to the elevator to provide an accurate position measurement for the data acquisition system.

LDV System. Vertical particle velocities were measured with a TSI laser Doppler velocimetry system mounted on a fixed table. The system used a Lexel 4W argon ion laser tuned to 514.4 nm with optical components configured in a backscatter mode. The final lens had a focal length of 2.2 m allowing sufficient removal of the system from the hot particle curtain. This application of LDV was unconventional because of the large particle sizes, and attention to the diameter-to-fringe spacing ratio was required. A detailed discussion of the LDV system can be found in Hruby and Burolla (1984).

Data Acquisition System. The data required from this experiment were particle temperature, air temperature, particle velocity, and spread of the particle curtain, all as functions of fall height (the distance from the hopper discharge slit). A Hewlett Packard 9816 computer, 3497A scanner, and 3456A digital voltmeter were used to acquire most of this information. Data collected with the computer system included weights from the scale, voltages from the thermocouples, frequencies from the LDV counter, voltages from the position transducer, and time from the HP 9816 internal clock.

Particle curtain dimensions were acquired by taking still photographs of a roughly eight inch square region of the falling curtain at various drop heights. Both front and edge views of the curtain falling at high and low mass flow rates were filmed with the particles at room temperature (particle temperature was not expected to affect spread). Width and depth measurements were scaled from the photographs to give approximate spread-versus-fall height data.

Experimental Procedure

Preparation. Master Bead™ particles were heated in a convection oven at the selected temperature for a minimum of five hours prior to running an experiment. The hopper was preheated for a minimum of one hour. The hopper temperature was set slightly cooler than the temperature of the convection oven to compensate for heat loss in transferrring particles from the oven to the hopper. After the hopper was filled with particles and positioned, data collection began.

Data Collection. Experiments were run using one of two routines. For the first routine, the hopper was fixed at the top of its travel, about 3.5 m above the catch bin. The elevator stage with temperature probes was moved from top to bottom to sample at eight selected drop heights. Particle temperatures and air temperatures were measured using this routine.

Because the particle velocity measurement (LDV) system could not be traversed vertically, the second routine required moving the hopper rather than the elevator to acquire particle velocity as a function of height. For each run, the hopper was positioned to give the desired drop height between the hopper and the fixed position of the LDV laser. The temperature probe platform was also fixed at the LDV height, and a repeat set of particle temperature data was gathered along with velocity values.

The step-by-step procedure of the two routines was similar. First, the hopper and elevator were positioned. The hopper door was opened and the particle sampling cup was inserted and held centered in the particle curtain. About ten seconds was allowed for equilibration of the curtain and the various thermocouples; then the computer sampling program was triggered. Data from the digital scale, position transducer, clock, plus hopper slit and sampling cup thermocouples were collected in about two seconds. Eight values from each thermocouple were taken and averages and standard deviations were calculated.

Depending on the routine, either air temperature or particle velocity was measured next. For air temperatures, the thermocouple rake was inserted immediately after withdrawing the sampling cup. While the rake was held centered in the cur-

tain, the computer collected eight values from each thermocouple. For velocity measurements, the computer collected and averaged forty values as soon as the particle sampling cup was withdrawn and the laser aperture opened.

When these measurements were complete, the hopper door was shut and the elevator or hopper was positioned for a subsequent run. A set of runs for eight different drop heights comprised one experiment and took from five to nine minutes to complete.

Three parameters were varied for the different experiments: collection routine, initial particle temperature, and mass flow rate. As discussed above, there were two collection routines. Three initial particle temperatures were used: room temperature (isothermal), 603 K, and 773 K. Finally, mass flow rate was set at either 0.02 kg/s or 0.04 kg/s. At least two experiments were run at each permutation of these three parameters.

Uncertainty. Some aspects of the chosen procedure and apparatus introduced uncertainty in the experimental results. First, as discussed above, the particle velocity measurement routine involved changing the overall fall height of the particle curtain. This would not be expected to influence the results unless disturbances were propagated upstream. By comparing particle temperature measurements from the two different routines, it was shown that, in fact, altering the downstream conditions made no difference. Therefore, the only important length was the distance between the height of the hopper door and the elevation where the measurements were made; total fall heights and conditions below the measurement location were not important.

Another source of uncertainty with respect to particle temperature was the use of the particle sampling cup due to its thermal mass and possible flow disturbance. Thermal mass effects were shown to be negligible by good agreement of hopper exit temperatures with sampling cup temperatures taken just below the exit. Since the sampling cup disturbed only the downstream flow, this effect was negligible for the reasons discussed above.

Numerical Analysis

A model of dilute gas-particle flows with heat and mass transfer has been developed by Crowe et al. (1977). The model (PSI-Cell, i.e., Particle Source in Cell) includes two-way mass, momentum, and thermal coupling between the phases and has been applied to simulations of spray drying (Crowe, 1980), electrostatic precipitators (Eschbach and Stock, 1979), cyclone separators (Crow and Pratt, 1974), and combustion (El-Bainhawy and Whitelaw, 1980). The PSI-Cell code was modified for the present study by including buoyancy in the air and temperature dependent properties of the air and the particles. A single particle radiation model was also included in the particle energy equation. Briefly, the PSI-Cell code consists of a steady, two-dimensional planar or axisymmetric, elliptic, Eulerian description of the gas flow field coupled with a Lagrangian description of the particle flow field. The gas flow field is determined using TEACHT (Gosman and Pun, 1973), which solves the conservation equations on staggered control volumes with the pressure, density, and temperature evaluated at control volume centers and the velocities evaluated at the control volume faces. A two equation (κ-ϵ) model of turbulence is included with constants established for a forced flow (Launder and Spalding, 1972). Convection and diffusion of a dependent variable are combined into a single term, which when integrated over the control volume, represents the flux of that variable across the faces of the control volume. These terms are evaluated using hybrid differencing (Spalding, 1972). This differencing scheme is a combination of central differencing and upwind differencing, switching from central to upwind when the absolute value of the cell Reynolds number is greater than two.

Gas Equations. The integrated forms of the conservation equations for mass, momentum, and energy with a planar geometry are given by:

$$(\rho u)_w^e \cdot \Delta y + (\rho v)_s^n \cdot \Delta x = 0 \tag{1}$$

$$\left(\rho uu - \mu_{\text{eff}} \cdot \frac{\partial u}{\partial x}\right)_w^e \cdot \Delta y + \left(\rho vu - \mu_{\text{eff}} \cdot \frac{\partial u}{\partial y}\right)_s^n \cdot \Delta x$$

$$= (P_w - P_e) \cdot \Delta y + \rho g \cdot \Delta x \cdot \Delta y$$

$$+ \mu_{\text{eff}} \cdot \frac{\partial u}{\partial x}\bigg|_w^e \cdot \Delta y + \mu_{\text{eff}} \cdot \frac{\partial v}{\partial x}\bigg|_s^n \cdot \Delta x + S_p^x \tag{2}$$

$$\left(\rho uv - \mu_{\text{eff}} \cdot \frac{\partial v}{\partial x}\right)_w^e \cdot \Delta y + \left(\rho vv - \mu_{\text{eff}} \cdot \frac{\partial v}{\partial y}\right)_s^n \cdot \Delta x$$

$$= (P_s - P_n) \cdot \Delta x - \mu_{\text{eff}} \cdot \frac{\partial u}{\partial y}\bigg|_w^e \cdot \Delta y + \mu_{\text{eff}} \cdot \frac{\partial v}{\partial y}\bigg|_s^n \cdot \Delta x + S_p^y \tag{3}$$

$$\left[\rho uT - \left(\frac{k}{c_p}\right)_{\text{eff}} \cdot \frac{\partial T}{\partial x}\right]_w^e \cdot \Delta y + \left[\rho vT - \left(\frac{k}{c_p}\right)_{\text{eff}} \cdot \frac{\partial T}{\partial y}\right]_s^n \cdot \Delta x = S_p{}^T \tag{4}$$

where e, w, n, s indicate that the corresponding terms are to be evaluated at the east, west, north, and south faces of the control volume, and Δx and Δy are the control volume dimensions in the x and y directions, respectively. The reduction in the area of the gas phase on the control surface due to the presence of the particles is negligible. The dissipation term in the energy equation is small and has been neglected. The sign of the body force term for the x component of momentum is such that the coordinate system is oriented with the x direction aligned with gravity. The source terms, $S_p{}^x$, $S_p{}^y$, and $S_p{}^T$, refer to the momentum and energy added to the gaseous phase by the particles. Additional equations and relationships for the gas flow solution are:

(1) Pressure is determined using the SIMPLE procedure described by Patankar (1980) which is formulated to insure local continuity;

(2) Differential equations for turbulent kinetic energy, κ, and dissipation, ϵ, are solved as presented in Launder and Spalding (1972);

(3) Effective viscosity and conductivity are given by

$$\mu_{\text{eff}} = \mu + \mu_{\text{turb}} \tag{5}$$

$$\mu_{\text{turb}} = c_\mu \rho \kappa^2 / \epsilon, \quad c_\mu = 0.09 \tag{6}$$

$$\frac{k_{\text{eff}}}{c_p} = \mu_{\text{eff}}. \tag{7}$$

Equation (7) is the result of assuming that the effective Prandtl number is unity. The influence of the particles on the effective viscosity and conductivity of the air is neglected.

(4) An ideal gas equation of state is used and Sutherland law relationships for the dependence of viscosity and thermal conductivity on temperature are prescribed (White, 1974).

Particle Equations. The particle velocity is calculated assuming that the aerodynamic drag and the gravitational body force are responsible for the motion; that is, the flow is dilute. This assumption is justified based on the fact that the particle volume fraction is on the order of 10^{-2} at distances greater than 10 cm from the hopper exit slit, and the particle volume fraction decreases substantially as the particles accelerate and the curtain widens.

The particle momentum and energy equations are given by

$$\rho_p \cdot \frac{\pi d_p^3}{6} \cdot \frac{Du_p}{Dt} = 3\pi d_p \mu \lambda (u - u_p) + \rho_p \cdot \frac{\pi d_p^3}{6} \cdot g \tag{8}$$

$$\rho_p \cdot \frac{\pi d_p^3}{6} \cdot \frac{Dv_p}{Dt} = 3\pi d_p \mu \lambda (v - v_p) \tag{9}$$

$$\rho_p c_{p_{part}} \cdot \frac{\pi d_p^3}{6} \cdot \frac{DT_p}{Dt} = \mathrm{Nu} k_f \pi d_p (T - T_p) - \epsilon \sigma \pi d_p^2 (T_p^4 - T_\infty^4) \tag{10}$$

where $\lambda = C_D \mathrm{Re}/24$, and Re is the particle Reynolds number based on the free stream properties and relative velocity. The radiative loss term represents the radiative heat transfer from an isolated particle and is a conservative estimate of the radiative heat loss. The particle energy equation is based on a uniform particle temperature which is justified by the fact that the Biot number for particles in the experiment is less than 0.1 (Incropera and DeWitt, 1981).

The drag coefficient used in the model corresponds to the steady state drag coefficient for an isolated sphere. The empirical equation used is

$$C_D = \frac{24}{\mathrm{Re}_f}(1 + 0.15\mathrm{Re}_f^{2/3}) \tag{11}$$

where Re_f is the Reynolds number based on the film temperature (which is the average of the particle temperature and the bulk air temperature) and the relative velocity between the particle and the air. This equation was developed for isothermal conditions with Reynolds numbers up to 10^3 (Clift et al., 1978). The effects of pressure gradient and particle acceleration on the drag coefficient are negligible because the material density ratio between the air and particles is less than 10^{-3}. Tsuji et al. (1982) found that the drag of a particle is unaffected by neighboring particles if the particle separation distance is ten or more diameters. This condition is met over the greater portion of the particle's trajectory in the falling curtain. The effect of turbulence on drag coefficient is difficult to quantify because turbulence intensity data are unavailable. If it is assumed that the root mean square of the turbulence generated by the particle is the product of the particle diameter and vortex shedding rate, a relative turbulence intensity of 0.1 is calculated (Clift, et al., 1978). At this value and at the relative Reynolds number of the falling particles, the effect of turbulence on the particle drag coefficient is minimal. Thus the expression used for λ is equations (8) and (9) becomes

$$\lambda = (\nu_f/\nu)(1 + 0.15\mathrm{Re}_f^{2/3}) \tag{12}$$

where ν is the kinematic viscosity and the nonsubscripted value corresponds to free stream conditions.

The Ranz-Marshall correlation is used for the Nusselt number, namely (Bird et al., 1960)

$$\mathrm{Nu} = 2 + 0.6\mathrm{Re}_f^{1/2}\mathrm{Pr}_f^{1/3}. \tag{13}$$

The effect of neighboring particles on the Nusselt number is not included. There are no data available to assess this effect but it is presumed small because the effect of neighboring particles on the drag coefficient is small.

Gas Source Terms. The force in the x direction on the gas in the computational cell due to the particles is given by:

$$S_p{}^x = \sum_i F_{p,i}^x \dot{N}_i \Delta t_i \tag{14}$$

where $F_{p,i}^x = 3\pi dp\mu\lambda(u_p - u)$ is the aerodynamic force on the gas due to a particle, $\dot{N}_i$ is the particle number flow rate, and Δt_i is the particle transit time across the cell, all for the ith trajectory. The sum is applied over every trajectory passing through the computational cell for which the source term is being evaluated. A similar expression holds for the y direction source term. The energy equation source term for the gas is given by:

$$S_p{}^T = \sum_i (Q_{p,i}/c_p)\dot{N}_i \Delta t_i \tag{15}$$

where $Q_{p,i} = Nuk_f \pi d_p (T_p - T)$ is the convection heat transfer rate from a particle to the air in the ith trajectory.

Initial Particle Conditions. As the particles flowed from the hopper in the experiment, there was a component of the particle velocity in both the horizontal and vertical directions. The (small) horizontal component, which arose due to either particle-particle collisions within the hopper or the nature of the discharge from the hopper, was not measured. A range of initial horizontal velocities from 0.3 cm/s to 3.0 cm/s for the particle flow was provided in the calculation. This range in particle velocity was sufficient to reproduce the measured spread of the particle curtain (the measured spread was roughly 3 cm total at a 2 meter fall height). The particle mass flow rate was divided into ten parts, with each part representing the same fraction of the total flow rate. These parts were distinguishable only by different initial conditions on particle velocity. Each part was given an initial temperature corresponding to the measured temperature in the hopper just above the discharge slit. The particles were considered to be spherical, with a uniform size of 650 μm, density of 3130 kg/m^3, and a specific heat that was a function of temperature (1057 J/kgK at 603 K).

Calculational Procedure. The calculations were performed in a vertical cylinder or channel, depending upon whether axisymmetric or planar geometry was considered. Symmetry was assumed about the cylinder (channel) centerline with the solution obtained over half of the cylinder (channel). The cylinder (channel) was 1.5 meters in radius (half-width) and 4.0 meters high. The particles were introduced at the top of the cylinder (channel) near the centerline with initial downward velocity and temperature as given in the previous section. Although the experiment did not have confining walls, the convergence of the calculations and the specification of boundary conditions for the elliptic equations is aided by the addition of a solid boundary. The effect of the outer wall on the results for particle velocity and temperature when the radius (half-width) of the cylinder (channel) was varied from 1.0 to 2.0 meters was less than 5 percent. Slightly larger changes of approximately 10 percent occurred in the air temperature. The computational mesh consisted of 20 axial grid lines (in the direction of fall of the particles) and 16 lateral grid lines. The grid spacing was non-uniform in both directions with the smallest axial grid spacing (4 cm) at the top of the cylinder (channel) near the particle source and the smallest lateral grid spacing (2 cm) at the symmetry axis and within the particle curtain. Since the spread of the particle curtain was only a few centimeters, the computations did not yield detailed information on the distribution of the temperature and velocity of the air within the curtain nor was this information available from the results of the experiment. The sensitivity of the calculated results to the grid size was determined to be less than 1 percent for particle velocity and temperature and less than 5 percent for air temperature when the number of grid lines was doubled in both directions.

The calculations were initiated by assuming a stagnant air field. The particle trajectories were calculated and the source terms evaluated. The gas flow equations were solved incorporating the particle source terms which gave rise to motion in the gas flow field (entrainment). The particle trajectories were recalculated and the source terms re-evaluated. The gas flow field was calculated again and the cycle was continued until

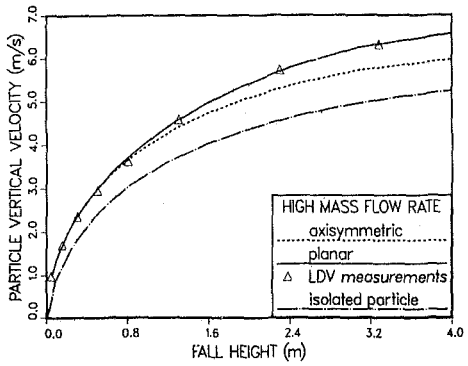

Fig. 7 Numerical prediction and experimental data of particle velocity in isothermal particle-air flow. (Uncertainty in velocity: ±0.25 m/s, Uncertainty in fall height: ±0.01 m at 20:1 odds.)

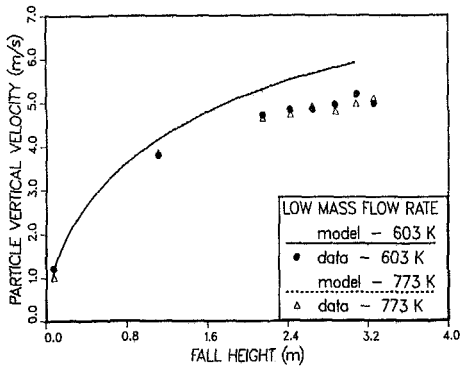

Fig. 8 Numerical prediction and experimental data of particle velocity in elevated particle temperature flow with low particle mass flow rate. The dashed and solid curves which represent the numerical results at different temperatures overlap. (Uncertainty in velocity: ±0.25 m/s, Uncertainty in fall height: ±0.01 m at 20:1 odds.)

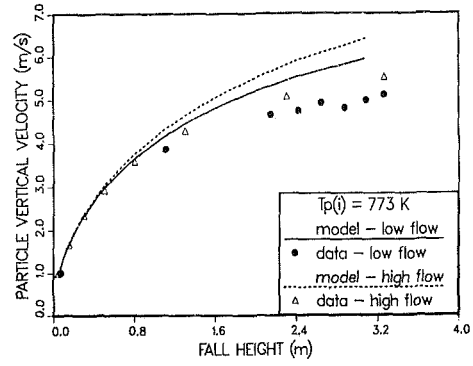

Fig. 9 Numerical prediction and experimental data of particle velocity in elevated particle temperature flow with two particle mass flow rates. (Uncertainty in velocity: ±0.25 m/s, Uncertainty in fall height: ±0.01 m at 20:1 odds)

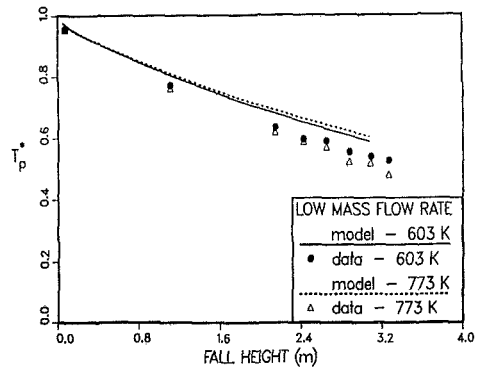

Fig. 10 Numerical prediction and experimental data of dimensionless particle temperature for low particle mass flow rate at two initial elevated particle temperatures. (Uncertainty in temperature: ±0.025 m/s, Uncertainty in fall height: ±0.01 m at 20:1 odds.)

convergence was achieved. This procedure took one to two minutes of computer time on the Cray-1.

Comparison of Experimental and Numerical Results

Unheated Flow Comparison. The geometry of the slit through which the particles exit the hopper was described earlier as being rectangular with an aspect ratio of 10:1. It was not clear that this aspect ratio was large enough to produce a purely two-dimensional, planar entrained air flow. Since the axisymmetric geometry allows for uniform air entrainment at a given distance from the axis of symmetry, both axisymmetric and planar geometries were used initially to determine which, if either, would result in acceptable agreement with particle velocity measurements made in the isothermal drop tests.

Figure 7 shows the results of the comparison between calculated and experimental vertical particle velocity as a function of distance from the hopper exit for the high mass flow rate of isothermal air-particle flow. Calculational results for both planar and axisymmetric geometries are shown. The results for the planar geometry are in excellent agreement with measurements whereas the axisymmetric results underpredict the data. Consequently, the planar geometry was used for all subsequent comparisons. Also shown in Fig. 7 is the result for a single isolated spherical particle falling in quiescent surroundings obtained by integrating equations (8)–(9) with air velocity components, u and v, set to zero. By comparison, particles in a curtain fall faster due to the entrainment of air which results in a downward component of air velocity in the curtain.

Heated Flow Comparison. Calculations of particle velocity and temperature, and air velocity and temperature have been made for the two mass flow rates and the two initial elevated particle temperatures. In this section, comparisons between calculations and experimental results are made for particle velocity, dimensionless particle temperature, and dimensionless air temperature. Although buoyancy effects for the air have been taken into account and a radiation heat loss term has been included in the particle energy equation, both of these effects are negligible for the conditions considered here.

Comparison of Particle Velocity. The calculated and measured vertical components of particle velocity as a function of distance from the hopper for the low mass flow rate and for the two initial particle temperatures (603 K and 773 K) are shown in Fig. 8. The effect of initial temperature on the predicted values is not discernible, and the effect on the measured values is small. The calculations overpredict the measured values of particle velocity.

Figure 9 shows the calculated and measured particle vertical velocity profiles for the two mass flow rates at the single initial particle temperature of 773 K. The calculations overpredict the velocity data for the high mass flow rate as well. The trend in both calculations and measurements toward higher particle velocities as the mass flow rate of particles increases is evident. The higher particle mass flow rate results in more air entrainment, increased downward air velocity in the curtain, and augmented particle fall velocities.

Comparison of Particle Temperature. For comparison

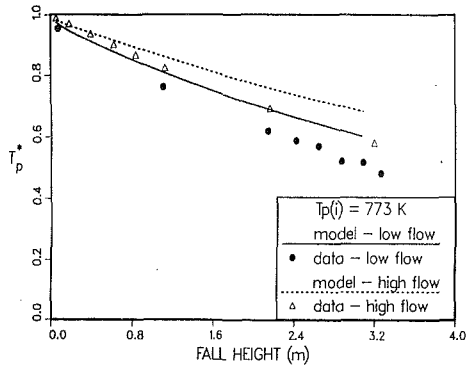

Fig. 11 Numerical prediction and experimental data of dimensionless particle temperature for two particle mass flow rates at an initial particle temperature of 773 K. (Uncertainty in temperature: ±0.025 m/s, Uncertainty in fall height: ±0.01 m at 20:1 odds.)

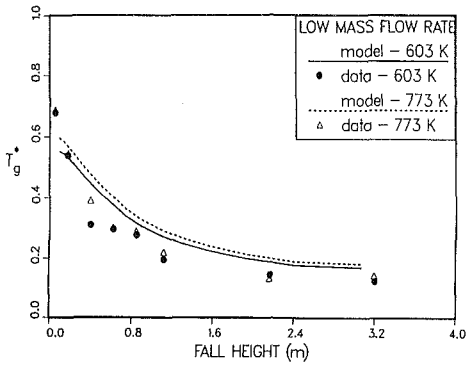

Fig. 12 Numerical prediction and experimental data of dimensionless air temperature for low particle mass flow rate at two initial elevated particle temperatures. (Uncertainty in temperature: ±0.07, Uncertainty in fall height: ±0.01 m at 20:1 odds.)

purposes, the particle temperature has been nondimensionalized: $T_p^* = (T_p - T_\infty)/(T_{po} - T_\infty)$. Dimensionless particle temperature is shown as a function of the distance from the hopper in Fig. 10 for the low mass flow rate case and for the two initial particle temperatures. The difference between the results for the two initial temperatures shown is quite small as a result of the nondimensionalization and the insignificance of radiative heat transfer. Calculations of particle temperature overpredict the measured values. This result indicates that the calculations underpredict the total heat transfer to the air.

Dimensionless particle temperature as a function of distance from the hopper for the two mass flow rates and for an initial particle temperature of 773 K is shown in Fig. 11. Both calculated and experimental results indicate that as the particle mass flow rate increases, the dimensionless particle temperature at a given fall height increases. The increase in dimensionless particle temperature at high mass flow rates is due to two factors; the increased particle concentration leads to a higher air temperature within the curtain and the increased relative particle velocity reduces the time available for heat transfer.

Comparison of Air Temperature. The measured and calculated dimensionless air temperature, $T_g^* = (T_g - T_\infty)/(T_{po} - T_\infty)$, is shown on Fig. 12 for the low mass flow rate case and for the two initial particle temperatures. The calculated air temperatures are higher than the measured values. The fact that the predicted air temperature is higher than measured does not necessarily imply that more energy was transferred to the air in the calculation; if this were true it would be inconsistent with the higher predicted than measured particle temperature. If the predicted air velocities are smaller than the experimental values, which were not measured, then the predicted air temperatures can be higher than those measured and still result in a smaller predicted than measured heat transfer to the air. As will be discussed in the next section, if the predictions were made with a particle drag coefficient that was too small then it is conceivable that predicted air velocities would be smaller than those in the experiment.

The variation of dimensionless air temperature as a function of distance from the hopper for the two mass flow rates and at the higher initial particle temperature is shown in Fig. 13. Both calculated and experimental values show an increase with increasing mass flow rate. This is expected since a higher mass flow rate of particles provides a larger source of heat to the surrounding air, and the air mass flow rate does not increase at the same rate as the particle mass flow rate.

Note that although both the particle and air temperature are decreasing as a function of distance from the hopper, it is not

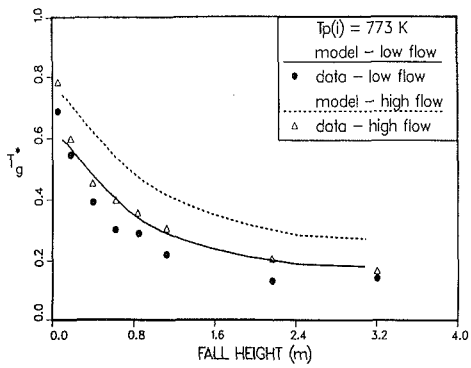

Fig. 13 Numerical prediction and experimental data of dimensionless air temperature for two particle mass flow rates at an initial particle temperature of 773 K. (Uncertainty in temperature: ±0.07 m/s, Uncertainty in fall height: ±0.01 m at 20:1 odds.)

true that the air is losing energy because a significant mass flow of air is occurring due to entrainment by the particles. For example, for the higher particle temperature and higher mass flow rate case, the downward mass flow rate of air at distances of 14, 89, and 191 cm from the hopper was calculated to be 0.054, 0.39, and 0.64 kg/s, respectively.

Drag Coefficient in Heated Flows

Because the calculations overpredict measured particle velocities in heated particle flows, the correlation used for the drag coefficient (equation (11)) needs to be examined in more detail. The calculations included the effect of hot particles by evaluating the Reynolds number of the film temperature in lieu of the bulk air temperature. This increased the calculated drag coefficient of a 650 μm particle at 773 K moving in air at 293 K with a relative velocity of 3 m/s by 70 percent from the value obtained assuming uniform air properties at 293 K. Still, the data suggest that the drag coefficient in hot particle flows is higher than predicted using the film temperature to determine the Reynolds number.

Very little information is available in the literature on the effect of surface-gas temperature difference on the particle drag coefficient. An analytic study by Kassoy et al. (1966) predicted that the drag coefficient of a particle in the Stokes flow regime would increase with increasing surface temperature and that the Nusselt number would decrease. The same trends result from the use of the film temperature to evaluate the air properties. There appears to be no analytic solution available for

temperature effects in the Reynolds number range of interest in this study ($10 < Re_f < 100$).

Some experimental studies have been reported in the Russian literature on the effect of particle surface temperature on particle drag coefficient. Babiy and Ivanova (1965) propose that the increased drag coefficient of burning particles is due solely to the increased surface temperature of the particle. They further propose that the drag coefficient should be correlated with a Reynolds number based on the surface temperature, not the average film temperature. They correlated a large volume of experimental data and proposed the following empirical relationships

$$C_D = \frac{52}{Re_s} (0 < Re_s < 50) \tag{16}$$

$$C_D = \frac{2}{Re_s^{0.2}} (Re_s > 50) \tag{17}$$

where Re_s is the Reynolds number evaluated using the kinematic viscosity of the gas at the particle surface temperature. This correlation leads to a lower drag coefficient than the one used in this study in the range $40 < Re_s < 120$. The particles falling in the curtain are in this range over the greater portion of their trajectory which leads to an even higher velocity if Babiy and Ivanova's correlation is used. Calculations were also done using Re_s instead of Re_f in the standard drag coefficient correlation given by equation (11) but the increase in drag was insufficient to account for the lower velocity observed in the experimental data.

Basina and Maksimov (1970) point out that the coal particles used in Babiy and Ivanova's correlations were not spherical and that the increased drag may partially be due to the asphericity. They carried out an experiment to measure the drag coefficient of a heated, 2.5 mm diameter spherical particle suspended in a horizontal stream of cooler air over a Reynolds number range of 1 to 150. They showed that the drag coefficient for heated particles was larger than the standard drag coefficient. The increase was as much as 45 percent for a particle at 723 K with a Reynolds number of 15, the effect decreasing with increasing Reynolds number to 26 percent at a Reynolds number of 40. This effect is attributed partially to increased viscous effects in the boundary layer as noted by Babiy and Ivanova, and partially to free convection effects. At low flow velocities they noted a vertical velocity component induced by free convection effects which probably had a significant effect on the measured drag coefficient. They point out that their data is only valid for a similar flow configuration (horizontal flow in a pipe). In the case of freely falling particles, the air velocities induced by free convection would increase the gas-particle relative velocity, and the effect of free convection on the drag coefficient would be greater.

Good agreement between the numerical and the experimental results for particle velocity in nonisothermal flows was obtained when the constant multiplying $Re^{2/3}$ in the drag coefficient of equation (11) was increased from 0.15 to 0.40, an increase of 166 percent. Because the calculated results for particle and air temperature also agreed well with the experimental results for particle and air temperature when the above change was made to the particle drag coefficient, the discrepancy between measured and predicted particle and air temperatures can be primarily associated with uncertainty in the particle drag coefficient and not the particle heat transfer correlation.

Conclusions

An experiment has been performed to determine the flow characteristics and the convective heat transfer in a curtain of freely falling particles. Measurements of particle velocity in heated and unheated flow at two mass flow rates have shown that the particles in a curtain fall faster than an isolated particle in free fall. Further, particle temperature measurements have shown that particle temperature at a given fall height is higher as the particle mass flow rate increases. Calculations using the PSI-Cell computer code, which accounts for the two-way momentum and thermal coupling between the particles and the air, are in excellent agreement with the particle velocity measurements in isothermal air-particle flow. The predictions show the same trends as the measurements for particle velocity, particle temperature, and air temperature in nonisothermal, heated particle flow. For the nonisothermal cases, these quantities are overpredicted. By using a larger drag coefficient, the predictions of particle velocity, particle temperature, and air temperature are in better agreement with experimental data. The data suggest that an increased drag coefficient should be used in flows where the particles are hot compared to the air. The convection coefficient for a single particle seems sufficient to describe the energy exchange in a dilute particle curtain when the local conditions are known.

Acknowledgment

This work was supported by the U.S. Department of Energy under contract DE-AC04-76DP00789.

References

Babiy, V. I., and Ivanova, I. P., 1965, "Aerodynamic Resistance of a Particle in a Nonisothermal Condition (in Russian)," Teploenergetika, Vol. 9, pp. 19–23.

Basina, I. P., and Maksimov, I. A., 1970, "Effect of Nonisothermicity on the Aerodynamic Drag of a Spherical Particle," *Heat Transfer-Soviet Research*, Vol. 2, No. 6, pp. 69–75.

Bird, R. B., Stewart, W. E., and Lightfoot, E. N., 1960, *Transport Phenomena*, Wiley, p. 409.

Brewster, B. S., and Seader, J. D., 1984, "Measuring Temperature in a Flowing Gas-Solids Suspension with a Thermocouple," *AIChE Journal*, Vol. 30, No. 4, pp. 676–679.

Burolla, V. P., Hruby, J. M., and Steele, B. R., 1984, "High Temperature Solar Thermal Energy Absorption with Solid Particles," *Proc. IECEC*, Vol. 3, pp. 1663–1668.

Clift, R., Grace, J. R., and Weber, M. E., 1978, *Bubbles, Drops and Particles*, Academic Press, New York.

Crowe, C. T., and Pratt, D. T., 1974, "Analysis of the Flow Field in Cyclone Separators," *Computers and Fluids*, Vol. 2, pp. 249–260.

Crowe, C. T., Sharma, M. P., and Stock, D. E., 1977, "The Particle-Source-in Cell (PSI-CELL) Model for Gas-Droplet Flows," ASME JOURNAL OF FLUIDS ENGINEERING, pp. 325–332.

Crowe, C. T., 1980, "Modeling Spray-Air Contact in Spray-Drying Systems," *Advances in Spray Drying*, Hemisphere Publishing, Chapter 3, pp. 63–99.

El-Bainhawy, V., and Whitelaw, J. H., 1980, "The Calculation of the Flow Properties of a Confined Kerosine-Spray Flame," *AIAA Journal*, Vol. 18, No. 12, pp. 1503–1510.

Eschbach, E. J., and Stock, D. E., 1979, "Optimization of Collection Efficiency by Varying Plate Spacing with an Electrostatic Precipitator," *Proceedings of the 2nd EPA Conference on Transfer and Utilization of Particulate Control Technology*, Denver.

Evans, G., Houf, W., Greif, R., and Crowe, C., 1986a, "Gas-Particle Flow Within a High Temperature Solar Central Receiver including Radiation Heat Transfer," *Journal of Solar Energy Engineering*, accepted for publication.

Evans, G., Houf, W., Greif, R., and Crowe, C., 1986b, "Numerical Modeling of a Solid Particle Solar Receiver," Sandia National Laboratories, SAND85-8249.

Gosman, A. D., and Pun, W. M., 1973, "Calculation of Recirculating Flow," Lecture Notes, Imperial College of Science and Technology, London, England.

Houf, W. G., and Grief, R., 1985, "Radiation Transfer in a Solar Absorbing Particle Laden Flow," *Radiation Heat Transfer*, ASME HTD-Vol. 43, eds. Armaly, B. F., and Emery, A. F., pp. 9–14.

Hruby, J. M., and Burolla, V. P., 1984, "Solid Particle Receiver Experiments: Velocity Measurements," Sandia National Laboratories, SAND84-8238.

Hruby, J. M., and Steele, B. R., 1986a, "A Solid Particle Central Receiver for Solar Energy," *Chemical Engineering Progress*, Vol. 82, No. 2, February, 1986.

Hruby, J. M., 1986b, "A Technical Feasibility Study of a Solid Particle Solar Central Receiver for High Temperature Applications," Sandia National Laboratories, SAND86-8211.

Incropera, F. P., and DeWitt, D. P., 1981, *Fundamentals of Heat Transfer*, Wiley, New York, p. 184.

Kassoy, D. R., Adamson, T. C., and Messiter, A. F., 1966, "Compressible Low Reynolds Number Flow Around a Sphere," *The Physics of Fluids*, Vol. 9, No. 4, pp. 671–681.

Launder, B. E., and Spalding, D. B., 1972, *Mathematical Models of Turbulence*, Academic Press.

Martin, J., and Vitko, J., 1982, "ASCUAS: A Solar Central Receiver Utilizing a Solid Thermal Carrier," Sandia National Laboratories, SAND82-8203.

Patankar, S. V., 1980, *Numerical Heat Tranfer and Fluid Flow*, McGraw-Hill.

Radosevich, L. G., 1985, "Final Report on the Experimental Test and Evaluation of the 10 MWe Solar Thermal Central Receiver Pilot Plant," Sandia National Laboratories, SAND85-8015.

Spalding, D. B., 1972, "A Novel Finite-Difference Formulation for Differential Expressions Involving Both First and Second Derivatives," *Int. J. of Numerical Methods Eng.*, Vol. 4, pp. 551–559.

Tsuji, Y., Morikwa, Y., and Terashima, K., 1982, "Fluid Dynamic Interaction Between Two Spheres," *Int. Journal of Multiphase Flow*, Vol. 8, No. 1, pp. 71–82.

Wallis, G. B., 1969, *One-Dimensional Two-Phase Flow*, McGraw-Hill.

White, F. M., 1974, *Viscous Fluid Flow*, McGraw-Hill.